Mode II Delamination Toughness of Z-Pinned Laminates

Wenyi Yan[a,b], Hong-Yuan Liu[a,*] and Yiu-Wing Mai[a]

[a]Centre for Advanced Materials Technology (CAMT), School of Aerospace, Mechanical and Mechatronic Engineering J07, The University of Sydney, Sydney, NSW 2006, Australia

[b]Computational Engineering Research Centre, Faculty of Engineering and Surveying, University of Southern Queensland, Toowoomba, QLD 4350, Australia

Abstract

Mode II delamination toughness of z-pin reinforced composite laminates is investigated using the finite element (FE) method. The z-pin pullout process is simulated by the deformation and breakage of non-linear springs. A critical shear stress criterion based on linear elastic fracture mechanics is used to simulate crack growth in an end-notched flexure (ENF) beam made of z-pinned laminates. The mode II toughness is quantified by the potential energy release rate calculated using the contour integral method. This FE model is verified for an unpinned ENF composite beam. Numerical results obtained indicate that z-pins can significantly increase the mode II delamination toughness of composite laminate. The effects of design variables on the toughness enhancement of z-pinned laminates are also studied, which provide an important technological base and useful data to optimise and improve the z-pinning technique.

Keywords: B. Fracture (delamination) toughness; C. Laminates; C. Delamination; C. Computational simulation; Z-pin reinforcement.

(Published in Composites Science and Technology)

[*]Corresponding author (Fax: 61 2 9351 7060; Email: liu_hy@aeromech.usyd.edu.au)

1. Introduction

Advanced composite laminates have been extensively used in many structural applications, especially in aerospace engineering due to their strength/weight ratio relative to metallic materials. Traditional fibre composites are manufactured by stacking together a number of plies, in which the fibres are orientated to provide in-plane reinforcement. A direct result of this process is that no fibres are positioned across the thickness of the laminate. Interlaminar delaminations, either mode I opening fracture or mode II shearing fracture, become the most common failure modes in composite laminates. A successful solution to these problems is to provide through-thickness reinforcement to the laminated composites because bridging by fibres in the thickness direction imposes direct closure tractions to the delamination crack-faces. Over the last decade, many techniques have been developed to enhance the strength of composite laminates in the thickness or z-direction. Among them, a novel approach, so-called z-pinning, has been recently developed by Foster-Miller Inc in the USA [1]. In this technique, short fibres initially contained in foam are inserted into the composite through a combination of heat and pressure compacting the foam. The z-pinning technique is proven to be a cost-effective method to improve the delamination toughness of composite laminates.

In the last few years, many experiments on modes I and II delaminations were conducted on composite laminates with z-pin reinforcement by Partridge and co-workers at Cranfield [2]. Their results show that the z-pin reinforcement indeed significantly improves the fracture toughness. In our recent work, the delamination toughness of z-pinned laminates under mode I loading was studied by explicitly simulating mode I crack growth using the finite element (FE) method [3]. Good agreement is achieved between the predicted results and experimental data.

Experiments to examine the toughness enhancement mechanisms by through-thickness fibres can be found in [4, 5]. To enable better physical understanding of the effectiveness of z-pin reinforcement, Timoshenko's beam theory was applied to study through-thickness reinforced

double-cantilever-beams (DCB) under mode I delamination. Jain and Mai [6] investigated the interlaminar mode I fracture reinforced by through-thickness stitching. They developed the first micro-mechanics model to describe fibre pulling out from the stitched DCB. The pullout force was then smeared over the stitch-induced bridging zone and was entirely due to the interface friction between stitches and composite laminate. In recent work by Liu and Mai [7], the bridging force of the z-pin is calculated by a fibre pullout model, which includes the whole pullout process: elastic deformation before z-pin debonding, elastic deformation and frictional sliding during debonding growth and finally frictional sliding. The discrete bridging forces calculated from this pullout model were then applied on the beams. The deformation of the DCB *versus* applied load was numerically quantified with Timoshenko's beam theory.

Jain and Mai [8, 9] have also studied mode II fracture toughness of stitched laminated End-Notched-Flexure (ENF) specimens by using first-order shear deformation laminated plate theory and beam theory. In the case of stitching, the bridging force comes from the elastic stretching of the threads. The bridging force was smeared over the bridging zone in their model. The bridging traction could be better dealt with by considering discrete distributed bridging forces especially in the case when the distance between stretching threads is large compared to the beam thickness. However, in doing so, it could be difficult to obtain an analytical closed form solution. Same theories and similar approaches have been applied by Massabo et al [10, 11] to examine a bridged mode II delamination in detail from an analytical and conceptual viewpoint. For example, they have discussed two limiting crack configurations: the small-scale bridging limit when the bridging zone size is constant and much smaller than the crack length; and the ACK limit when the critical applied shear stress is independent of crack length.

The present research is intended to establish a FE model to quantify the effects of z-pins on the delamination toughness under mode II loading condition. The FE method is robust, which can overcome some limitations of the beam theory or shear deformation plate theory so that both short-crack and long-crack specimens can be analysed by the FE method. Shear deformation, material orthotropy and geometrical non-linear large deformation can be easily

included in a FE study by using commercial FE packages. In our FE model, the bridging traction from the effective z-pins is simulated individually along the bridging zone. The energy release rate from linear elastic fracture mechanics is applied to quantify the delamination toughness. Detailed FE simulations are given in Section 2, which includes the simulation of z-pin pullout, the contour integral method to calculate the potential energy release rate and the application of the critical shear stress criterion. This established FE model is then verified by benchmarking predicted numerical results against theoretical solutions for the unpinned ENF laminate. Numerical results of z-pinned ENF laminated composites are finally presented in Section 3.

2. Approaches to Delamination of Z-Pinned Composite Laminates

2.1 Configuration and material data

In this work, a finite element model is developed to study the mode II delamination toughness of z-pinned composite laminates. Since the End-Notched-Flexure (ENF) beam is commonly accepted as a standard test to evaluate the delamination toughness of composite laminates subjected to mode II failure [12], the present theoretical study will focus on the ENF test on z-pinned laminates. Figure 1 shows a schematic of the ENF test geometry for z-pin reinforced composite laminate. Z-pins are inserted in the laminates along the z direction. An initial crack with length a_0 was created in the mid-plane of the laminate. The distance of the nearest column of z-pins to the crack-tip is a_p. The distribution of the z-pins can be described by four parameters: n_c, n_r, d_c and d_r. n_c is number of columns of pins arranged in x-direction and n_r is number of rows of pins arranged in y-direction. d_c is spacing between neighbouring z-pin columns; and d_r is spacing between neighbouring z-pin rows. With increasing the applied force $2P$ at the mid-point of the beam, a delamination crack will grow along the mid-plane. It has been proven that truly mode II fracture can be obtained in ENF tests [12] for the unpinned laminates. In the present case of z-pinned laminates, mode II fracture will still dominate the delamination process, which is discussed below.

Cartie and Partridge [2] carried out ENF tests to study mode II delamination behaviour of z-pinned composite laminates. In their tests, the z-pins were made from carbon fibre/BMI composite rods and the laminates from unidirectional IMS/924 composite, which was considered as an orthotropic material in our simulation. The material constants and geometrical parameters used in our FE calculations are based on their test results, which are summarized in Tables 1 and 2.

E_1 and E_2 are Young's moduli in *x*- and z-direction, respectively. ν_{12} is Poisson's ratio, which characterizes compression in *z*-direction due to the tension applied along *x*-direction. μ_{12} is shear modulus for planes parallel to the co-ordinates *xOz*. *h* is half-thickness, *w* width and *L* half-length of the ENF specimen.

2.2 Toughness analysis

According to linear elastic fracture mechanics, the toughness of a material/structure can be quantified by the energy release rate, *G*, which is defined as [13]

$$G = \frac{1}{w}\left(\frac{dU_e}{da} - \frac{dU_s}{da}\right), \tag{1}$$

where *w* is width of the crack front, (here, the width of the ENF specimen), *a* is crack length, U_e is external work performed and U_s is stored elastic energy. The potential energy release rate *G* represents the energy available for the creation of a unit new crack area.

For an unpinned ENF specimen, the dissipated energy is entirely consumed by the surface energy of the newly created crack under mode II loading, which is denoted by G_c. During delamination crack growth, G_c must be equal to the intrinsic mode II toughness, G_{IIC}, of the composite laminate. Hence,

$$G = G_c = G_{IIC}. \tag{2}$$

For a z-pinned ENF specimen, the dissipated work includes not only the crack surface energy but also those dissipated during the z-pin pullout process, which includes the elastic energy of

the pins, the debonding work between pins and laminate, and friction work consumed during pullout. Thus, the total potential energy release rate of a z-pinned ENF specimen, G, which at equilibrium equals G_R, the crack-resistance, consists of two parts: specific energy for the new crack surface, G_c, and specific energies due to z-pin pullout, G_p, which depends on the extent of delamination growth, Δa. That is,

$$G = G_R = G_c + G_p(\Delta a) \tag{3}$$

and $G_c = G_{IIC}$. Therefore, the delamination toughness of z-pinned laminates can be completely described by the total energy release rate, that is, the crack-resistance, G_R. The FE method is applied to analyse G_R of z-pinned ENF specimens.

2.3 Pullout model and pullout simulation

Z-pin pullout from laminated composites is a very complex process. Figure 2 is a schematic of the pullout process of a z-pin caused by mode II delamination. During delamination the crack faces move relative to each other along the crack growth direction with a displacement 2δ at the location of the pin. Consequently, the pin is forced to pull out of the laminate. We assume a predominant tensile force T exists in the pin, which is the total axial force of a pin against the pin/laminates interfacial shearing and bending. Experiments on ENF by Cartie [14] indicated that the delaminated crack faces were kept open during mode II crack growth. Thus, the friction effect between the crack faces is not included in the model. This crack opening displacement originates from the bending of the pins at the ends that are being pulled out as shown in Fig. 2. Since the opening is very small and crack growth is predominantly mode II, bending of the z-pins is neglected in our study. Under mode II shearing, T acts roughly along the crack surfaces in x-direction and its amplitude varies with relative pullout displacement 2δ during the pullout process. Hence, the pullout model can be described by the functional relation below:

$$T = f(\delta), \tag{4}$$

which can be determined from experiments. The effect of different pullout models on mode I delamination in a DCB has been investigated by Liu *et al.* [15]. In the present theoretical and

numerical study, a simple bi-linear function is adopted, which is

$$T = \begin{cases} \dfrac{T_a}{\delta_a}\delta, & 0 \le \delta \le \delta_a \\ T_a - \dfrac{T_a}{h-\delta_a}(\delta - \delta_a), & \delta_a \le \delta \le h \end{cases} . \tag{5}$$

This function is shown in Fig. 3 (a), in which the pullout force increases rapidly towards a peak value T_a at $\delta=\delta_a$ and then it decreases gradually to zero at $\delta=h$ on complete pullout from the laminates with a half-thickness equal to h, Fig. 1.

Eq. (5) or Fig. 3(a) represents the mode II bridging law where the pin bends and then pulls out completely. Depending on the materials, from which the pins and composite laminate are made, the z-pins in an ENF test may break before being completely pulled out [2]. In the case of pin breakage, the pin may fracture at or after the peak force of the pullout curve shown in Fig. 3(b) and Fig. 3(c), respectively.

In our numerical study, the case of pin pulling out completely, which is the case of Eq. (5) or Fig. 3(a), is considered. However, from the numerical viewpoint, in principle, the approach developed here can also be applied to deal with the cases of pin breakage once the additional parametric values for T_b and δ_b in Fig. 3(b) and Fig. 3(c) are determined. We do, however, realize that there is numerical instability in such cases and techniques have been developed to overcome this problem such as by having a descending branch dropping from T_b at δ_b to zero load at a pullout distance only marginally larger than δ_b.

In our FE model, the pullout process of a pin from the composite laminates is simulated by a non-linear spring whose properties are described by Eq. (5). However, the peak bridging force per unit width, p_s, of a non-linear spring in plane stress is determined in our FE model by:

$$p_s = \frac{T_a n_r}{w}, \tag{6}$$

where n_r is number of rows of pins arranged along the width of the beam, that is, the *y*-direction in Fig. 1.

2.4 Contour integral

The energy release rate is calculated by the contour integral method. According to linear elastic fracture mechanics (see [13]), the potential energy release rate, *G*, is equal to a contour integral with the integrating path starting from the lower crack surface and ending at the upper crack surface, i.e.,

$$G = \int_{\Gamma} W_s dz - (T_x \frac{du_x}{dx} + T_z \frac{du_z}{dx}) dS , \tag{7}$$

where W_s is strain energy density of composite, T_x and T_z are components of the traction vector at the section dS of the contour Γ, u_x and u_z are displacement components.

The FE package ABAQUS adopts a domain integral method to numerically calculate the contour integral based on the divergence theorem. This method is proven to be quite effective in that accurate contour integral estimates can be obtained even with quite coarse meshes because the integral is taken over a domain of elements surrounding the crack front. Errors in local solution parameters have less effect on the domain integrated value, that is, the energy release rate [16]. Hence, it is not necessary to simulate the stress singularity near the crack-tip. Ordinary 4-node bi-linear plane stress elements are used in our FE analyses.

2.5 The critical shear stress criterion

To evaluate the crack-tip situation, a critical stress criterion can be used to assess whether the crack is at a critical state to grow or not. According to ABAQUS [16], the crack grows when the shear stress at a specified distance ahead of the crack-tip reaches a critical value under mode II loading condition. The stress field near the crack-tip can be determined by the energy release rate. Sih *et al* [17] studied the general crack problem in orthotropic materials. In the

mode II case, the relation between the energy release rate, G or G_{II}, and the shear stress, τ_{12}, ahead of the crack-tip is (see also Suo [18] and Poursartip et al. [19]):

$$\tau_{12} = \frac{1}{\sqrt{2\pi a_{11}}}\left(\frac{a_{11}}{a_{22}}\right)^{1/8}\left(0.5+\frac{2a_{12}+a_{66}}{4\sqrt{a_{11}a_{22}}}\right)^{-1/4}\frac{\sqrt{G_{II}}}{\sqrt{r}}, \tag{8}$$

where a_{11}, a_{22}, a_{12} and a_{66} are determined by material elastic constants. For the case of plane stress studied here, they are ([20])

$$a_{11} = \frac{1}{E_1}, \qquad a_{22} = \frac{1}{E_2},$$

$$a_{12} = -\frac{\nu_{21}}{E_2} = -\frac{\nu_{12}}{E_1}, \qquad a_{66} = \frac{1}{\mu_{12}}. \tag{9}$$

r in Eq (8) represents the distance from the crack-tip. Given the critical potential energy release rate of the composite laminate for mode II fracture, G_{IIC}, the shear stress ahead of the crack-tip at any location r can be obtained from Eq. (8). Here, the critical energy release rate, G_{IIC}, is considered a material constant.

By applying the critical shear stress criterion, the crack would advance if the shear stress at given location reaches the critical value, which is approximately equivalent to the energy release rate reaching the intrinsic mode II fracture toughness of the composite laminate. Because the shear stress is very close to the crack-tip and is in front of and not behind it, it can be treated as a local stress. The critical local stress value can approximately represent the toughness of the local composite even in a z-pinned laminate. Our numerical results have confirmed that the local shear stress distributions in front of the crack-tip are roughly identical for pinned and unpinned laminates during crack growth under this critical shear stress criterion.

To use the critical shear stress criterion to simulate crack growth, a basic requirement is to obtain an accurate stress value in front of the crack-tip. For this purpose, very fine meshes are established along the crack-growth path. In total, there are about 16,000 elements used in the

FE model. It takes about 26 h in a Compaq ES45 supercomputer with one CPU to finish a crack advance of 24 mm.

2.6 Model verification

The accuracy of the stress value in front of the crack-tip is verified first. The calculated shear stress ahead of the stationary crack tip from an unpinned ENF sample is shown in Fig. 4. These numerical results are compared with the analytical solution of Eq (8) from linear fracture mechanics. In both cases in which G_{II} equals 700 J/m^2 and 1000 J/m^2, respectively, the numerical results agree reasonably well with the analytical solutions, especially when r is less than 0.1 mm. Based on a critical stress at a critical distance fracture mechanics concept, a critical shear stress of 442 MPa at r=0.05 mm is adopted for crack growth corresponding to an intrinsic toughness G_{IIC} = 700 J/m^2 [14]. It should be noted that this critical stress value does not correspond to any physical property of the laminate but is a parameter used for crack growth modeling under mode II.

For an unpinned ENF beam, there are no z-pins to improve the delamination toughness of the composite laminates. In this case, an accurate solution for the potential energy release rate G_{II} of an ENF beam with a stationary crack is available (see, Hutchinson and Suo [21]). Based on this solution, for plane stress, we obtain:

$$G_{II} = \frac{9(Pa)^2}{4w^2h^3E_1}(1+Y\lambda^{-1/4}h/a)^2, \tag{10}$$

where $\lambda = a_{11}/a_{22}$. The dimensionless factor Y is approximated by:

$$Y(\rho) = 0.206 + 0.078(\rho-1) - 0.008(\rho-1)^2 \tag{11}$$

where $\rho = (a_{12}+0.5a_{66})/(a_{11}a_{22})^{1/2}$. Inserting the material parameter values to Eq. (10) gives the theoretical G_{II} results for crack lengths a=25 mm and a=30 mm in Fig. 5 represented by the two dotted curves. The two solid lines in the figure are obtained from our finite element simulations. Clearly, the FE results compare very well with the theoretical solutions.

For an unpinned ENF specimen, during crack growth, the energy release is only consumed in the creation of new crack surfaces. That is, $G_p = 0$ and Eq. (2) holds. The calculated energy release rate, *G*, from FE analysis using the contour integral method should give the same value as the critical energy release rate G_{IIC} used to calculate the critical shear stress during crack growth. Thus, FE analysis was first carried out to simulate crack growth in an unpinned ENF specimen. Figure 6 shows the variation of *G* with crack growth, Δa, for G_{IIC} = 700 J/m^2 and 1000 J/m^2, respectively. In both cases, the calculated *G* increases slightly in the initial crack growth region less than 20 mm, then it settles back to the expected values. These numerical results manifest the ACK limit as discussed in [10, 11]. When the crack growth exceeds this limit, the critical shear stress criterion can be accurately applied to simulate crack growth. Nonetheless, Fig. 6 indicates that the maximum deviation from the assumed G_{IIC} is about 15%. Since the enhancement of delamination fracture toughness by z-pins would be large enough to overshadow this overestimation, we consider this error to be acceptable and not affect the validity of our conclusions.

2.7 Dimensional analysis

Crack growth in z-pinned ENF specimens is fairly complex. Many parameters contribute to the failure processes and they can be studied effectively by using the dimensional analysis method. Generally, with given material elastic properties, the functional dependence of the crack-resistance, G_R, is:

$$G_R = g_1(P, \Delta a, a_0, a_p, w, h, G_{IIC}, T_a, \delta_a, n_c, d_c, n_r, d_r), \tag{12}$$

Since the applied force *2P* at the loading point also represents the toughness of the material/ structure, and is hence similar to G_R, it can be taken out from g_1. Thus, Eq. (12) becomes:

$$G_R = g_2(\Delta a, a_0, a_p, w, h, G_{IIC}, T_a, \delta_a, n_c, d_c, n_r, d_r). \tag{13}$$

For plane stress, the effect of row spacing, d_r, is neglected. Then, according to Eq. (6), the peak force in the springs, p_s, is determined by the product of the peak force of the single pin pullout model, T_a, and the number of z-pins in a row, n_r. Thus, in the parametric study, we only focus on the effect of T_a while keeping n_r fixed at 5 according to Cartie and Partridge [2]. Also, the initial crack length a_0 is 25 mm in our simulations. The effect of the z-pinned zone from the crack-tip, a_p, is implicitly included in crack growth Δa. Hence, a_p is also fixed as 2 mm in our analysis. With these assumptions, G_R is reduced to:

$$G_R = g_3(\Delta a, h, G_{IIC}, T_a, \delta_a, n_c, d_c) \tag{14}$$

and from dimensional theory [22], we obtain the dimensionless function g_4 as:

$$\frac{G_R}{G_{IIC}} = g_4\left(\frac{\Delta a}{h}, \frac{\delta_a}{h}, \frac{T_a}{G_{IIC}h}, \frac{d_c}{h}, n_c\right). \tag{15}$$

Thus, the normalized potential energy release rate of an z-pinned ENF specimen, G_R / G_{IIC}, is completely determined by the dimensionless crack growth, $\Delta a / h$; normalized location of the peak force in the z-pin pullout model, δ_a / h; normalized peak force, $T_a /(G_{IIC} h)$; normalized column spacing, d_c / h; and number of columns of pins, n_c. With Eq (15), the effects of all the parameters on mode II delamination toughness of z-pinned ENF specimens are studied in Section 3.

3. Results and Discussion

3.1 Enhanced delamination toughness due to z-pinning

As discussed in Section 2.3, the values of δ_a and T_a should be measured experimentally by well-designed z-pin pullout tests under mode II shearing conditions. Our current work on z-

pin pullout test under mode I tension [23] shows that the values of δ_a and T_a for mode I bridging law are affected by many factors, such as, material and geometry properties of the pin and laminates, interfacial bonding and friction stresses. So far, there are no experimental data published for z-pin pullout under mode II shearing. In this work, different assumed values are used in our FE simulations to calculate the delamination fracture in z-pinned ENF specimen. Figs. 7(a) and 7(b) show the crack-resistance G_R *versus* crack growth Δa curves computed from our FE analysis. In Fig. 7(a), three FE curves are illustrated with different values of T_a while keeping a constant δ_a of 0.01 mm; and in Fig. 7(b), three different values of δ_a are chosen for the FE curves with the same T_a of 180 N. The dotted curves represent the results for unpinned ENF samples. Here, the effect of z-pinning is clearly demonstrated in all the five cases with different T_a and δ_a. For example, as shown in Fig. 7(a) a maximum G_R of 2030 J/m^2 can be achieved in the case of T_a=200 N and δ_a =0.01 mm. This value is 2.9 times that of the unpinned value. Therefore, z-pinning is an effective technique to improve model II delamination toughness of composite laminates.

As mentioned above, Partridge and co-workers at Cranfield did many ENF tests to study the mode II fracture resistance of z-pinned composite laminates. For comparison, the measured G_R data for the same size and areal density of z-pins were extracted from Cartie [14] and re-plotted in Figs. 7(a) and 7(b). Clearly, almost all the test data overlap with our predicted G_R-curves suggesting that the selected T_a and δ_a values are reasonable for the z-pinned laminates.

3.2 Parametric study

To enable the optimal design of z-pinned composite laminates against mode II delamination, a parametric study on the dimensionless terms of Eq. (16) is performed in this section. Figure 8 shows the effect of the normalized pullout model parameter, δ_a/h, on the normalized energy release rate, G_R/G_{IIC}, during crack growth. Here, we consider three values of δ_a/h: 3.33×10^{-3}, 1.67×10^{-3} and 1.33×10^{-2}; and other parameters are fixed: n_c = 4, d_c/h = 2.33 and $T_a/G_{IIC}h$ = 61.9. It is seen that the normalized toughness G_R/G_{IIC} is higher at smaller δ_a/h, since a larger

z-pin pullout force is reached sooner at a shorter normalized crack length $\Delta a/h$. Physically, this implies that stiffer pins should be used to obtain smaller δ_a.

The effect of the dimensionless parameter, $T_a/G_{IIC}h$, is shown in Fig. 9 and is more dramatic than δ_a/h. For $T_a/G_{IIC}h$=95.24, the maximum G_R/G_{IIC} is about 1.84 and this becomes >4.0 for $T_a/G_{IIC}h$=285.7. For given values of G_{IIC} and h, this can be interpreted as due to the effect of the maximum pin pullout force T_a and hence the dissipation work in pulling out a pin, which is the area under the *T versus* δ curve in Fig. 3. In practice, the peak pullout force T_a can be made higher by improving the adhesion toughness between z-pins and composite laminate.

Figure 10 shows the influence of the number of z-pin columns n_c varying from 1 to 4 on the normalized G_R/G_{IIC} curves of z-pinned laminates. For a given column spacing d_c, the number of columns defines the size of the z-pinned zone. Hence, the results obtained are expected. The toughening effect is felt for longer crack lengths and the maximum toughness is higher if there are more columns of z-pins. Likewise, if we keep the column of pins constant, say n_c=4 as in Fig. 11, smaller column spacing, d_c/h, gives higher normalized toughness, G_R/G_{IIC}, over a shorter bridging length, $\Delta a/h$. This is a clear indication of the interactions between z-pin columns. The predictions are consistent with experimental results obtained by Cartie and Partridge [2], in which they increased the z-pin density (equivalent to decreasing the column spacing) and improved significantly the mode II delamination toughness of ENF specimens. Hence, it is practical to increase the pin density or decrease the column spacing in order to optimize the z-pinning technique.

4. Concluding remarks

A FE approach is developed to investigate the model II delamination toughness of z-pinned composite laminates in ENF tests. The effect of z-pins is studied with carefully arranged non-linear springs. A critical shear stress criterion is used to explicitly simulate crack growth in an ENF beam made up of z-pinned composite plies. The fracture toughness is quantified by the

potential energy release rate, which in turn is calculated by using the contour integral method. The FE model is verified with an ENF unpinned laminate. Our numerical results indicate that z-pins significantly increase the model II delamination toughness, which quantitatively agrees with available experimental data. Parametric studies indicate that the toughness can be improved by increasing the pullout peak force, number of z-pin columns; and by reducing the column spacing. These findings, together with our previous study on mode I delamination toughness [3], provide a set of useful guidelines for optimal design of z-pinning of composite laminates.

Acknowledgements

Supports by the Australian Research Council to WY (Research Associate), H-YL (Research Fellow) and Y-WM (Federation Fellow) are much appreciated. Some of the calculations were carried out at the National Facility of the Australian Partnership for Advanced Computing through an award under the Merit Allocation Scheme to WY.

References

1. Freitas G, Magee C, Dardzinski P, Fusco T. Fiber insertion process for improved damage tolerance in aircraft laminates. J Adv Mater 1994; 25(4): 36-43.
2. Cartie DDR, Partridge IK. Delamination behaviour of z-pinned laminates. In: *Proceedings of the 12th Iinternational Conference on Composite Materials*, ICCM12, Paris 5-9 July 1999.
3. Yan W, Liu H-Y, Mai Y-W. Numerical study on the mode I delamination toughness of Z-pinned laminates. Comp Sci Tech 2003;63:1481-1493.
4. Rugg KL, Cox BN, Massabo R. Mixed mode delamination of polymer laminates reinforced through the thickness by z-fibres. Composites Part A 2002; 33: 177-190.
5. Rugg KL, Cox BN, Ward KE, Sherrick GO. Damage mechanisms for angled through-thickness rod reinforcement in carbon-epoxy laminates. Composites Part A 1998; 29:1603-1613.
6. Jain LK, Mai Y-W. On the effect of stitching on mode I delamination toughness of laminated composites. Comp Sci Tech 1994; 51:331-345.
7. Liu H-Y, Mai Y-W. Effects of z-pin reinforcement on interlaminar mode I delamination. In: *Proceedings of the 13th International Conference on Composite Materials*, ICCM13, Beijing, 25-29 June 2001.
8. Jain LK, Mai Y-W. Analysis of stitched laminated ENF specimens for interlaminar mode II fracture toughness. Int J Frac 1994; 68:219-244.
9. Jain LK, Mai Y-W. Determination of mode II delamination toughness of stitched laminated composites. Comp Sci Tech 1995; 55:241-253.
10. Massabo R, Mumm DR, Cox, BN. Characterizing mode II delamination cracks in stitched composites. Int J of Frac 1998; 92:1-38.
11. Massabo R, Cox B N. Concepts for bridged mode II delamination cracks. J Mech Phys Solids 1999; 47:1265-1300.

12. Carlsson LA, Gillespie JW Jr. Mode-II interlaminar fracture of composites. In: Friedrich K editor. *Application of fracture mechanics to composite materials.* Chaper 4, pp.113-157, Amsterdam: Elsevier, 1989.
13. Williams JG. Fracture mechanics of anisotropic materials. In: Friedrich K editor. *Application of fracture mechanics to composite materials*. Chapter 1, pp. 3-38, Amsterdam: Elsevier, 1989.
14. Cartie DDR. Effect of z-fibres on the delamination behaviour of carbon fibre/epoxy laminates. PhD thesis, Cranfield Univeristy, U. K. 2000.
15. Liu H-Y, Yan W, Mai Y-W, Z-pin bridging force in composite delamination, In: B. R. K. Blackman BRK, Pavan A and Williams JG editors. *Fracture of Polymers, Composites and Adhesives II, ESIS Publication 32*, pp. 491-502, Amsterdam: Elsevier, pp. 491-502, 2003.
16. ABAQUS 2002 Version 6.3. Providence, RI: HKS Inc.
17. Sih GC, Paris PC, Irwin GR. On cracks in rectilinearly anisotropic bodies. Int J Fract Mech 1965; l:189-203.
18. Suo Z. Delamination specimens for orthotropic materials. ASME J Appl Mech 1990; 57:627-634.
19. Poursartip A, Gambone A, Ferguson S, Fernlund G. In-situ SEM measurements of crack tip displacements in composite laminates to determine local G in mode I and II. Engr Fract Mech 1998; 60:173-185.
20. Lekhnitskii SG. *Theory of elasticity of an anisotropic elastic body*. San Francisco: Holden-Day, Inc. 1963.
21. Hutchinson JW, Suo Z. Mixed mode cracking in layered materials. Advances in Applied Mechanics 1991; 29:63-191.
22. Anderson TL. *Fracture mechanics: Fundamentals and applications*. Second Edition, Boca Raton: CRC Press, 1995.
23. Dai S-C, Yan W, Liu H-Y and Mai Y-W. Investigation on z-pin bridging law by z-pin pullout test, submitted to Comp Sci Tech, 2003.

Table 1. Material constants of composite laminate.

E_1 (GPa)	E_2 (GPa)	ν_{12}	μ_{12} (GPa)
165	11	0.3	37.9

Table 2. Values of parameters to describe ENF and z-pinning.

h (mm)	w (mm)	L (mm)	a_0 (mm)	a_p (mm)	d_c (mm)	n_c	n_r
1.5	20	50	25	2	3.5	4	5

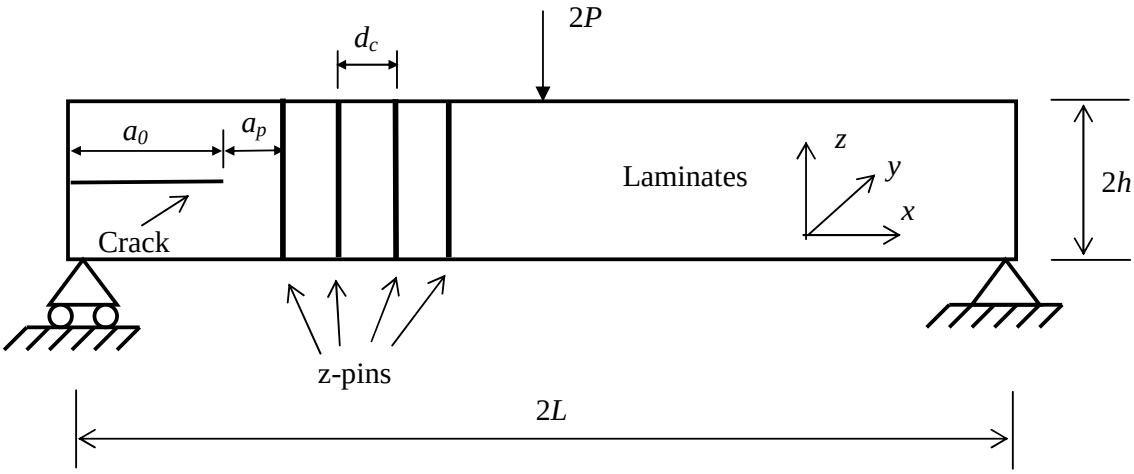

Figure 1. Illustration of a mode II delamination test for z-pin reinforced laminate: end-notched-flexure (ENF) geometry.

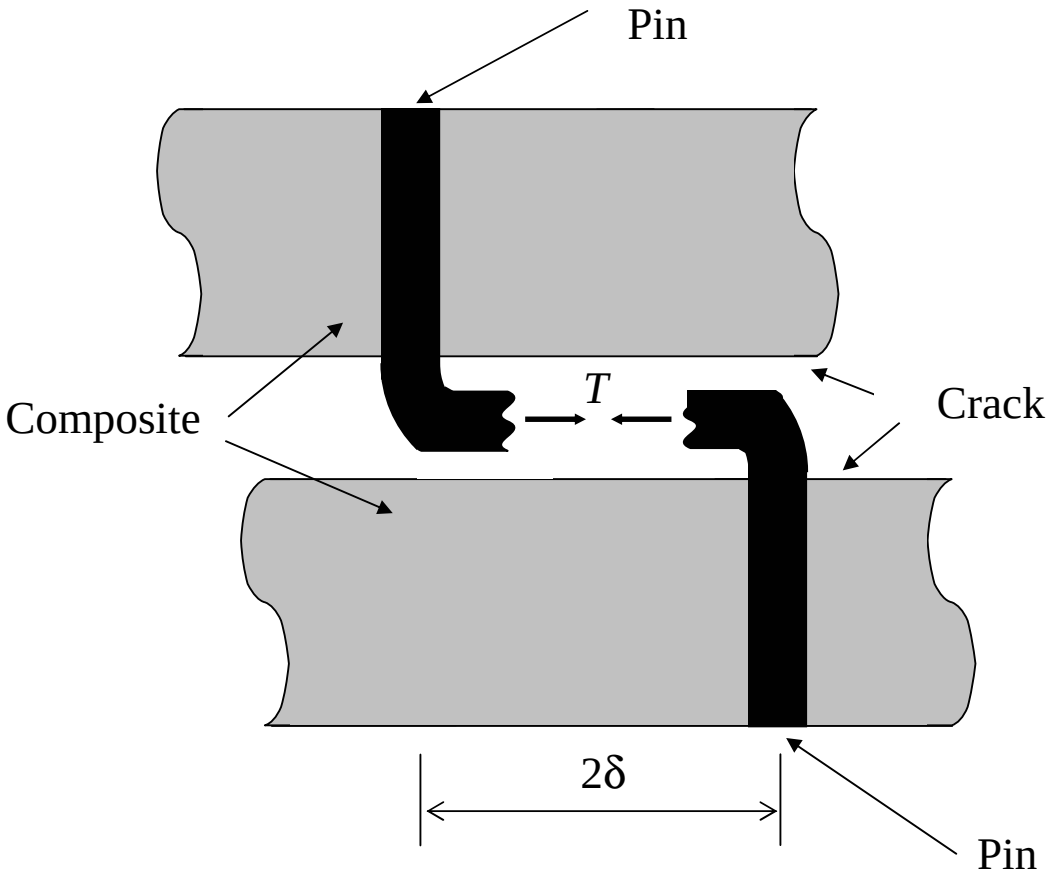

Figure 2. Schematic of the pullout of a z-pin under model II delamination.

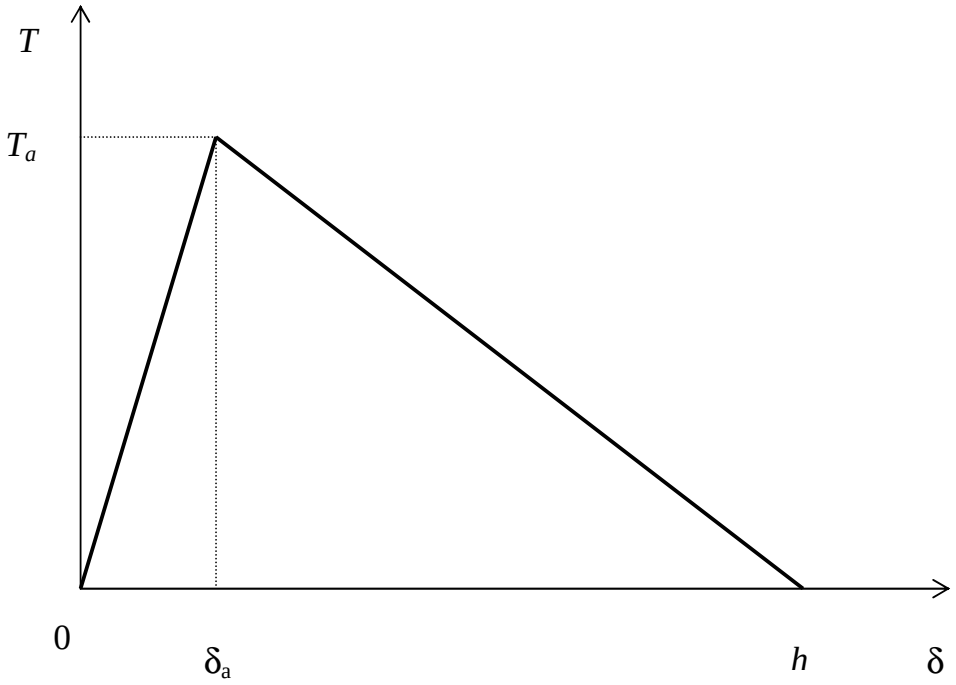

Figure 3(a)

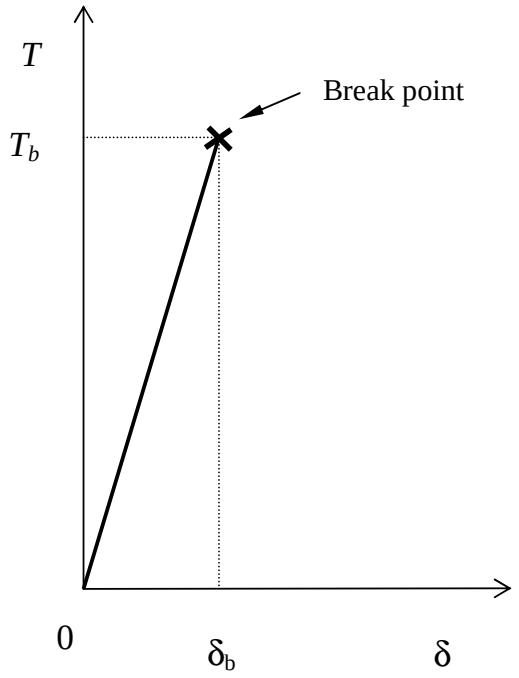

Figure 3(b)

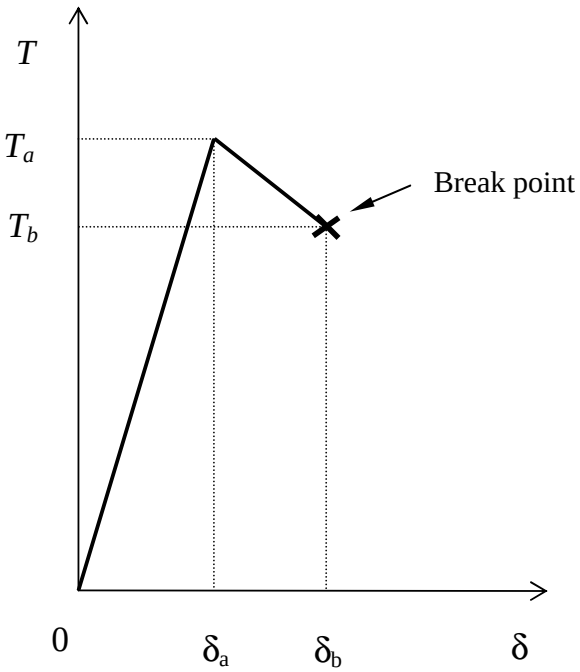

Figure 3(c)

Figure 3. (a) Schematic of mode II z-pin pullout model with pin completely pulled out, which is assumed in this study. (b) Schematic of mode II z-pin pullout model with pin breakage at the peak pullout force. (c) Schematic of mode II z-pin pullout model with pin breakage after reaching the peak pullout force.

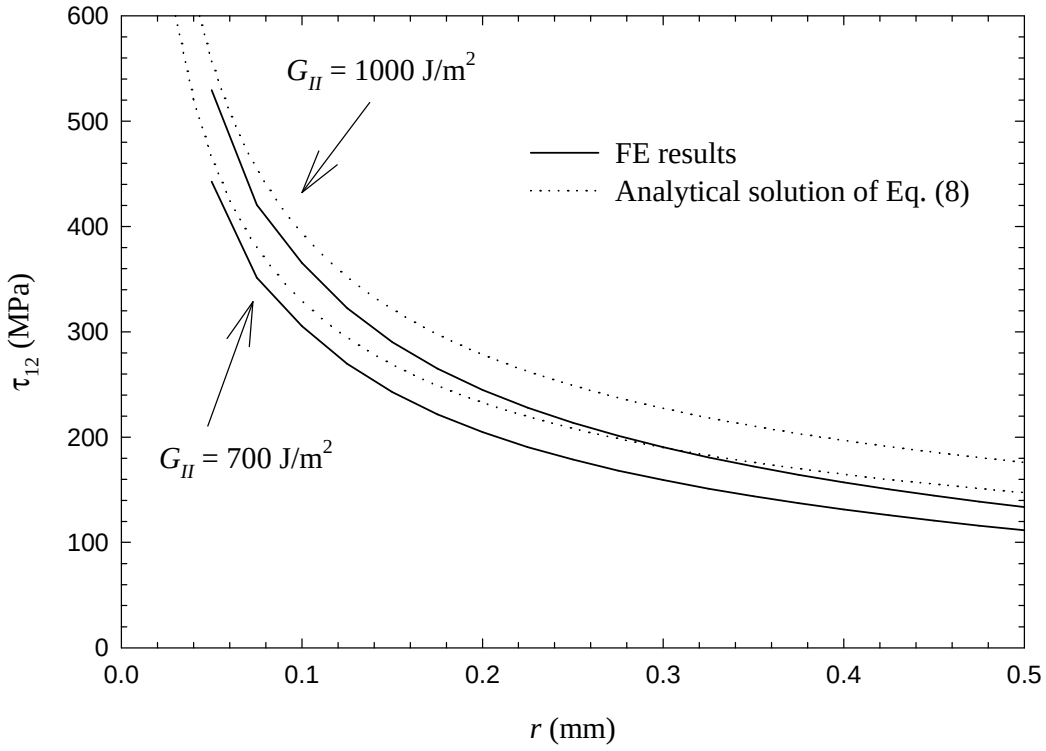

Figure 4. The variation of shear stress, τ_{12}, ahead of the crack-tip with applied energy release rates G_{II} = 700 J/m^2 and 1000 J/m^2, respectively.

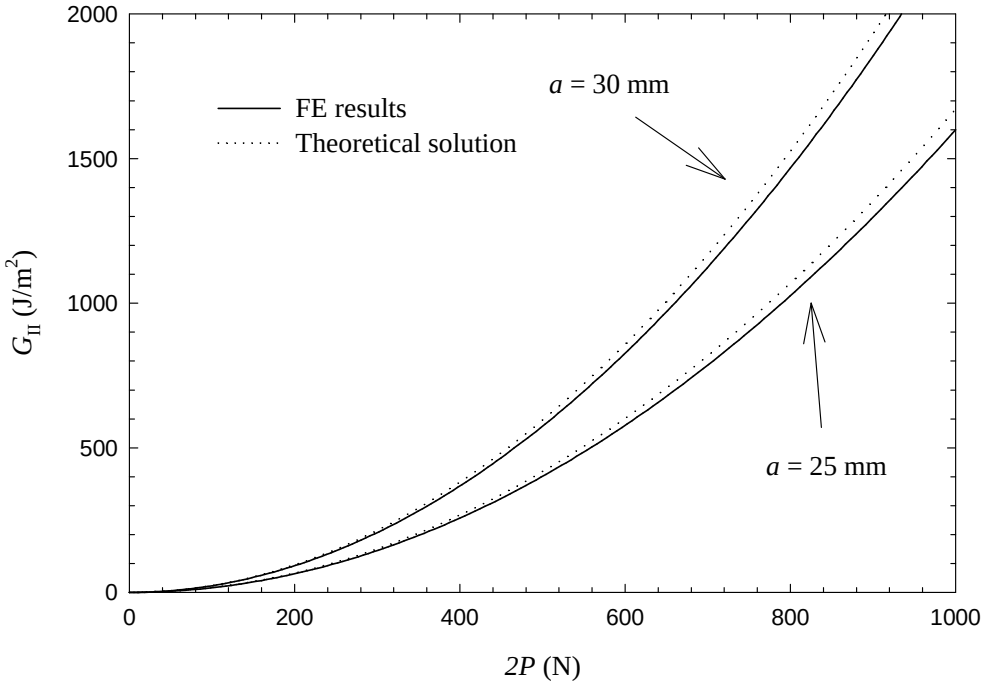

Figure 5. Variation of mode II energy release rate G_{II} versus applied force $2P$ for a = 25 mm and 30 mm.

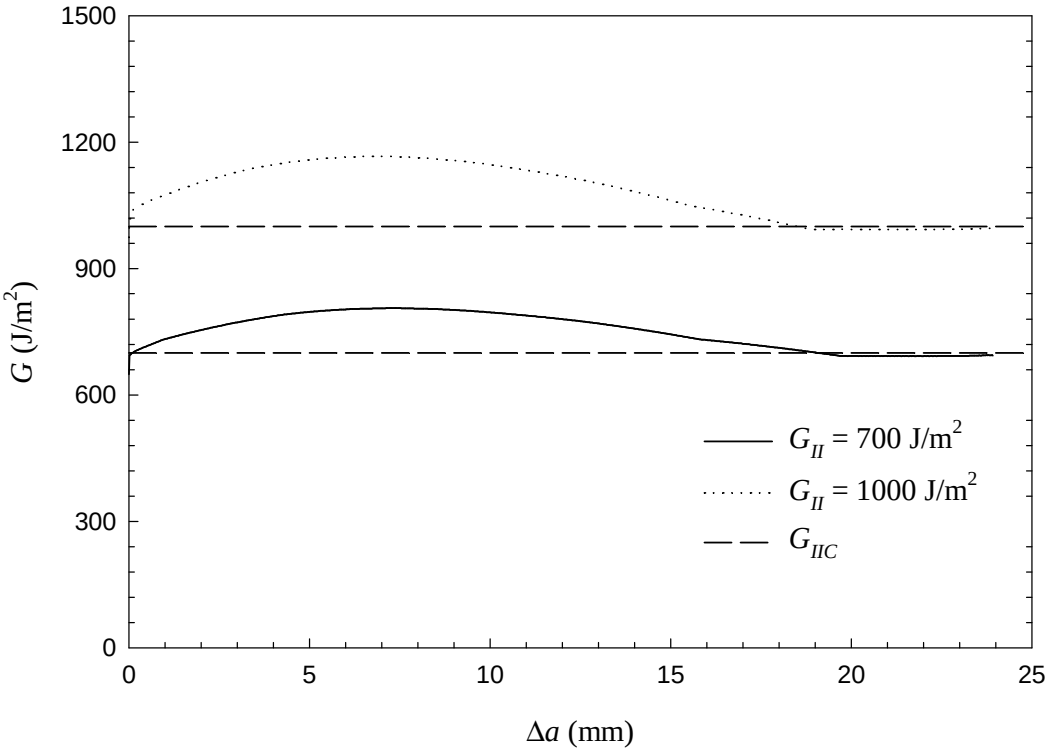

Figure 6. Calculated energy release rate G of an unpinned ENF specimen as a function of crack growth Δa for different critical energy release rates, G_{II} = 700 and 1000 J/m^2.

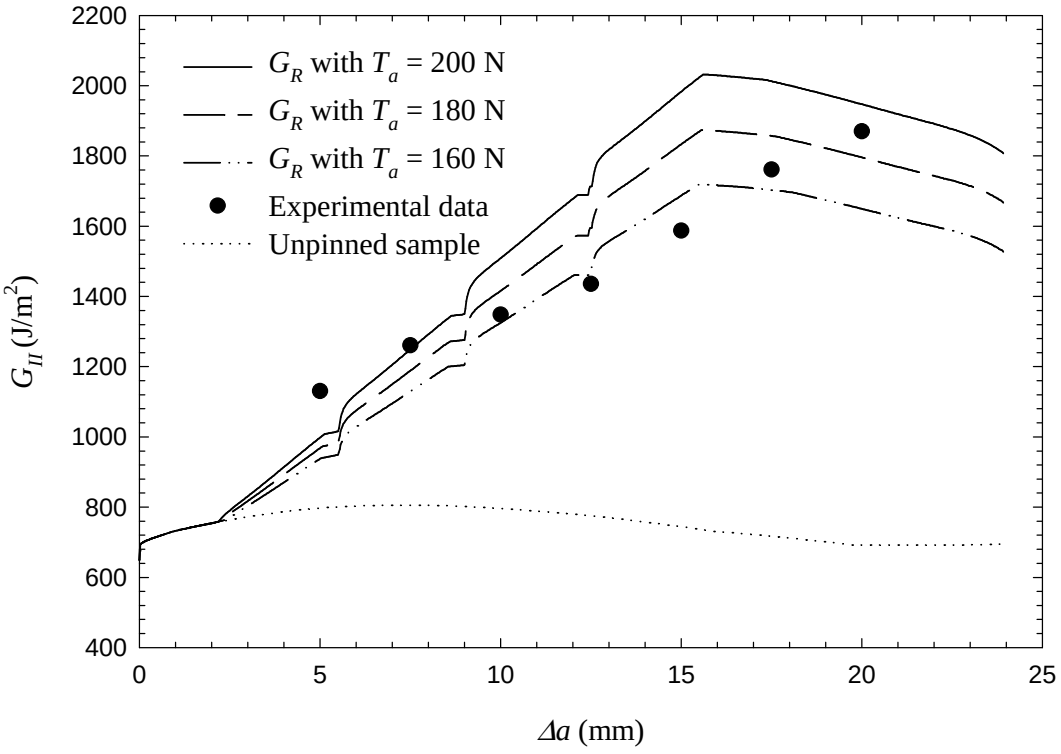

Figure 7(a). Predicted crack-resistance G_R curves of z-pinned ENF laminates *versus* crack growth Δa for different values of T_a while keeping constant δ_a of 0.01mm, compared to experimental data and an unpinned sample. (G_{IIC} = 700 J/m^2).

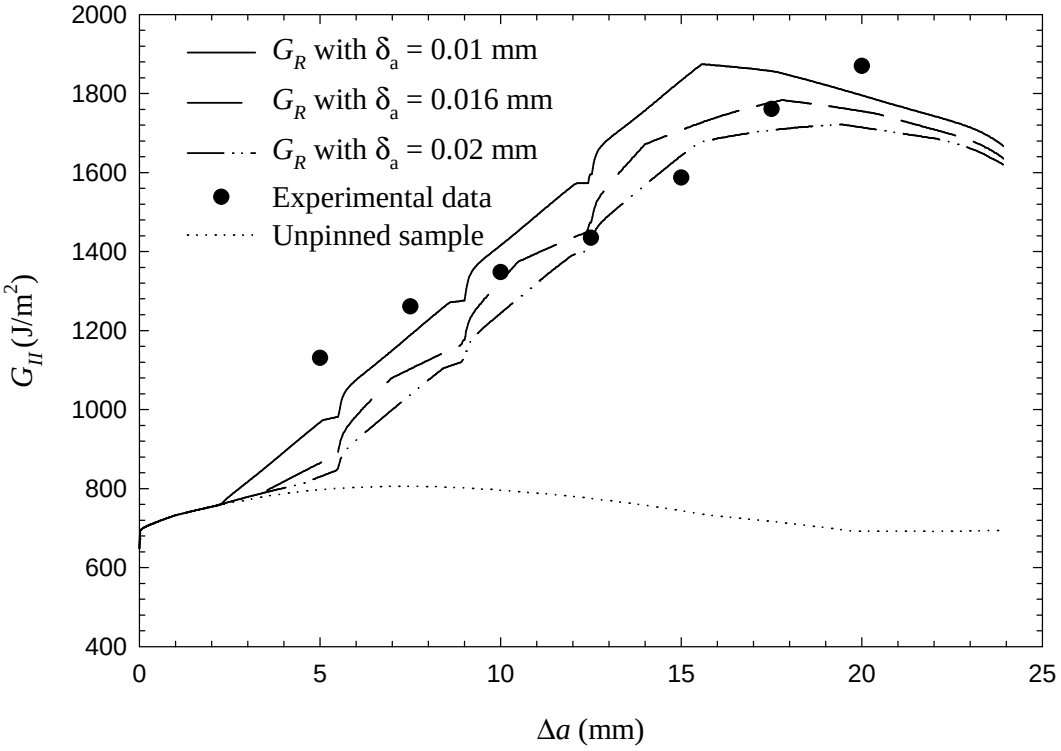

Figure 7(b). Predicted crack-resistance G_R curves of z-pinned ENF laminates *versus* crack growth Δa for different values of δ_a while keeping constant T_a of 180 N, compared to experimental data and an unpinned sample. (G_{IIC} = 700 J/m^2).

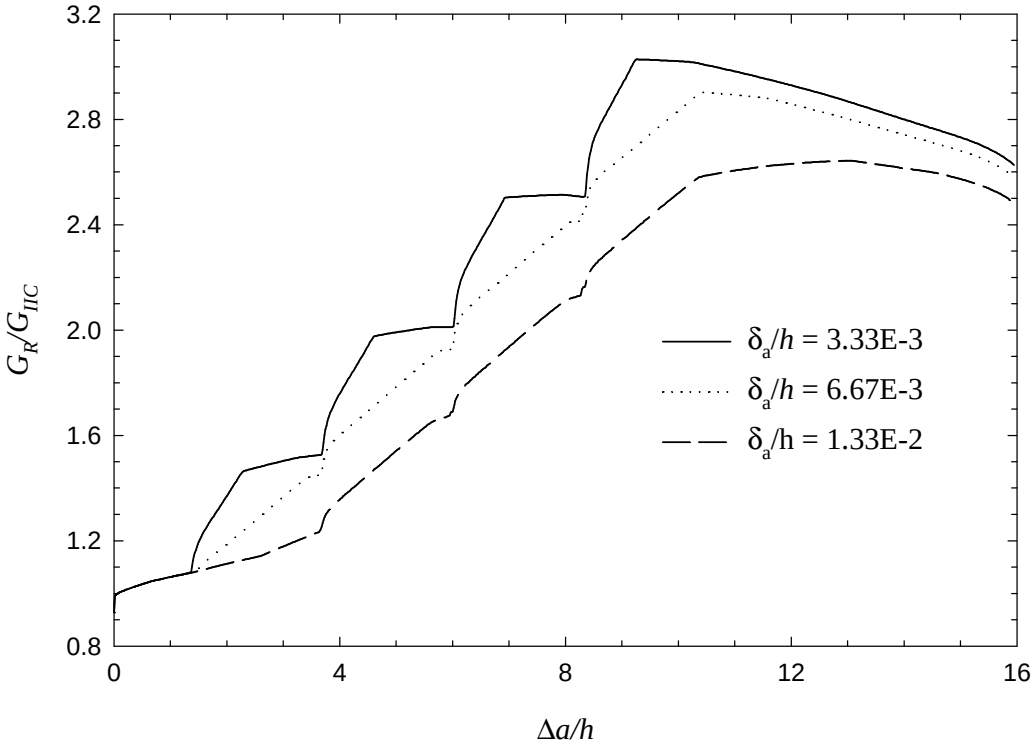

Figure 8. Influence of normalized pullout model parameter, δ_a/h, on normalized delamination toughness, G_R/G_{IIC}, during crack growth with $n_c = 4$, $T_a/G_{IIC}h = 190.5$ and $d_c/h = 2.33$.

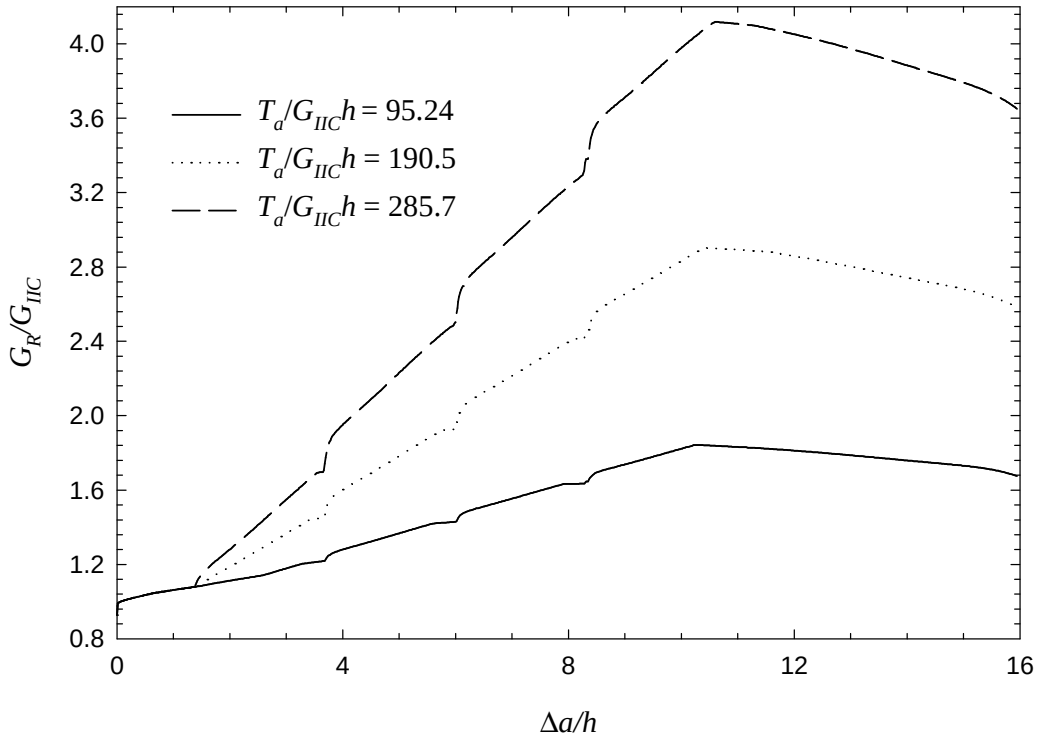

Figure 9. Influence of normalized pullout model parameter, $T_a/G_{IIC}h$, on normalized delamination toughness, G_R/G_{IIC}, during crack growth with $n_c = 4$, $\delta_a/h = 0.00667$ and $d_c/h = 2.33$.

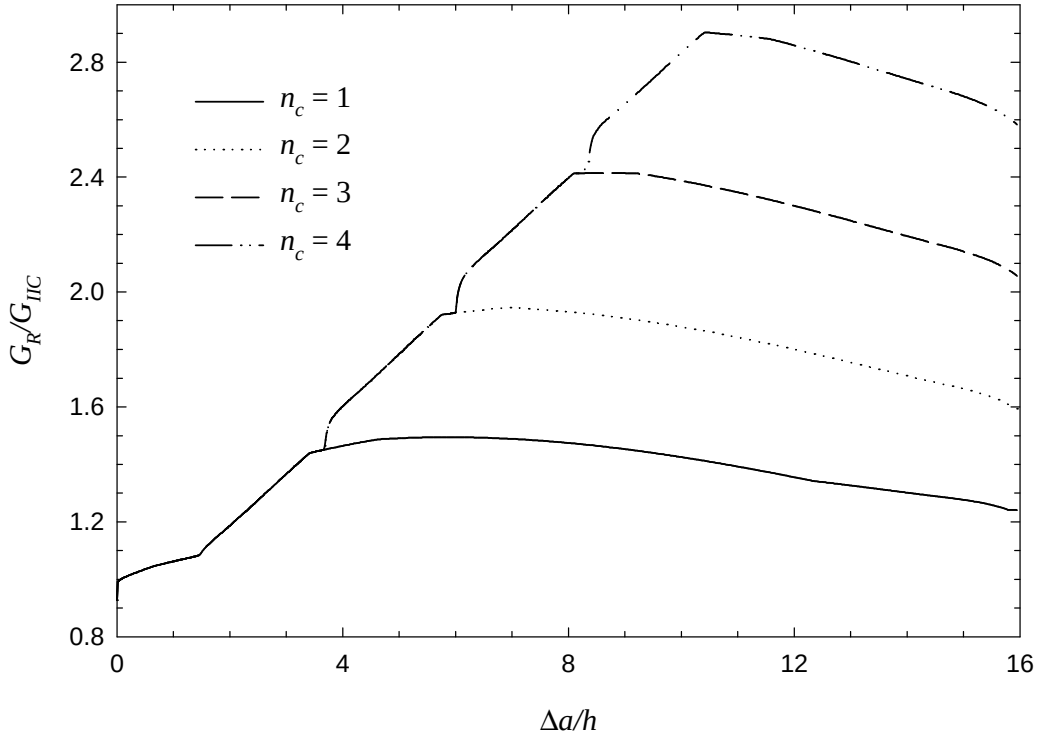

Figure 10. Influence of number of z-pin columns, n_c, on normalized delamination toughness, G_R/G_{IIC}, during crack growth with $T_a/G_{IIC}h = 190.5$, $\delta_a/h = 0.00667$ and $d_c/h = 2.33$.

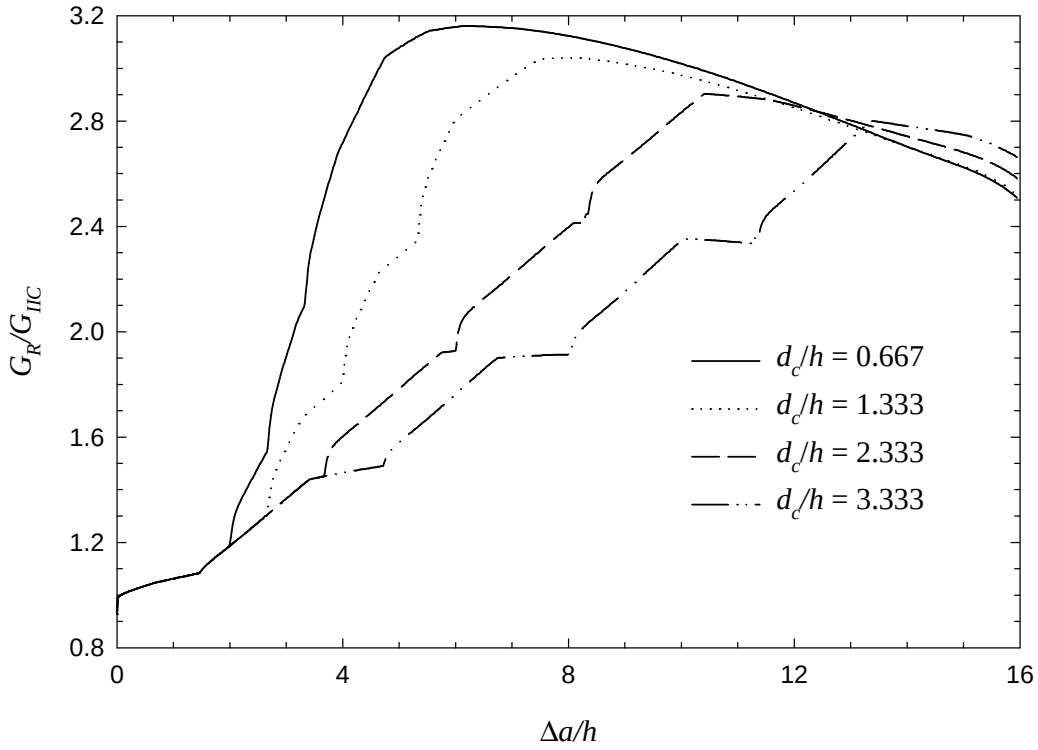

Figure 11. Influence of normalized column spacing, d_c/h, on normalized delamination toughness, G_R/G_{IIC}, during crack growth with $T_a/G_{IIC}h$ = 190.5, δ_a/h = 0.00667 and n_c = 4.